CCM2–CCM3 interaction stabilizes their protein expression and permits endothelial network formation

Kyle M. Draheim,[1]* Xiaofeng Li,[1]* Rong Zhang,[1] Oriana S. Fisher,[1] Giulia Villari,[1] Titus J. Boggon,[1] and David A. Calderwood[1,2]

[1]Department of Pharmacology and [2]Department of Cell Biology, Yale University, New Haven, CT 06520

Mutations in the essential adaptor proteins CCM2 or CCM3 lead to cerebral cavernous malformations (CCM), vascular lesions that most frequently occur in the brain and are strongly associated with hemorrhagic stroke, seizures, and other neurological disorders. CCM2 binds CCM3, but the molecular basis of this interaction, and its functional significance, have not been elucidated. Here, we used x-ray crystallography and structure-guided mutagenesis to show that an α-helical LD-like motif within CCM2 binds the highly conserved "HP1" pocket of the CCM3 focal adhesion targeting (FAT) homology domain. By knocking down CCM2 or CCM3 and rescuing with binding-deficient mutants, we establish that CCM2–CCM3 interactions protect CCM2 and CCM3 proteins from proteasomal degradation and show that both CCM2 and CCM3 are required for normal endothelial cell network formation. However, CCM3 expression in the absence of CCM2 is sufficient to support normal cell growth, revealing complex-independent roles for CCM3.

Introduction

Cerebral cavernous malformations (CCM) are devastating dysplasias of the vasculature. The disease occurs in familial and sporadic forms, both of which manifest predominantly in the central nervous system as dilated, thin-walled blood vessels that form mulberry-shaped lesions and are strongly associated with hemorrhagic stroke, epilepsy, seizure, and other focal neurological disorders (Chan et al., 2010). Even though the loss of any single CCM protein, CCM3 (cerebral cavernous malformations 3; PDCD10, programed cell death 10), CCM2 (cerebral cavernous malformations 2; malcavernin), or KRIT1 (K-rev interaction trapped 1; CCM1, cerebral cavernous malformations 1), results in overlapping disease phenotypes, the proteins have no sequence homology and are structurally distinct. CCM2 is thought to directly bind both CCM3 and KRIT1 (Voss et al., 2007; Draheim et al., 2014; Fisher and Boggon, 2014), which suggests that a CCM complex may have essential roles in normal endothelial function, and that disruption of the complex, by loss of any of the three proteins, may contribute to CCM disease. However, the basis for CCM complex formation and its functional significance remain unknown.

Animal and cellular studies have connected the CCM proteins to many endothelial cell functions including migration, polarization, and lumen formation, as well as angiogenic sprouting, branching, and maturation (Draheim et al., 2014). In a variety of settings, *CCM2* loss phenocopies many *KRIT1*-deficient phenotypes, particularly vascular defects (Chan et al., 2010). The CCM2–KRIT1 interaction has been shown to cross-stabilize both proteins (Faurobert et al., 2013), and similar signaling pathways are affected by loss of either protein (Hogan et al., 2008; Draheim et al., 2014; Fisher and Boggon, 2014). The CCM2–KRIT1 interaction is therefore considered to be intrinsic to CCM complex function. In contrast, the role of CCM3 within the CCM complex has yet to be determined. The best-characterized role of CCM3 is as a bridging factor within the striatin-interacting phosphatase and kinase (STRIPAK) complex, which is essential for cell polarity and migration (Goudreault et al., 2009; Kean et al., 2011; Fidalgo et al., 2012). The role of CCM3 in the STRIPAK complex is likely to be independent of the CCM complex (Kean et al., 2011). Interestingly, however, a CCM2

*K.M. Draheim and X. Li contributed equally to this paper.

Correspondence to Titus J. Boggon: titus.boggon@yale.edu; or David A. Calderwood: david.calderwood@yale.edu

Abbreviations used in this paper: CCM, cerebral cavernous malformations; FAT, focal adhesion targeting; FAT-H, FAT-homology; HHD, harmonin homology domain; NSLS, National Synchrotron Light Source; PTB, phosphotyrosine-binding; qPCR, quantitative real-time PCR; STRIPAK, striatin-interacting phosphatase and kinase.

The Rockefeller University Press $30.00
J. Cell Biol. Vol. 208 No. 7 987–1001
www.jcb.org/cgi/doi/10.1083/jcb.201407129

paralogue (CCM2L) that cannot bind CCM3 enables endothelial proliferation and competes with vascular stabilizing effects of CCM2 (Zheng et al., 2012), which is suggestive of the importance of the interaction between CCM2 and CCM3. There is therefore a need to delineate the specific role of CCM2's recruitment of CCM3.

Prior crystallographic studies showed that CCM3 contains an N-terminal dimerization domain and a C-terminal focal adhesion targeting (FAT)-homology domain. The CCM3 FAT-homology (FAT-H) domain contains an exquisitely conserved surface that was termed the hydrophobic patch 1 (HP1) site (Li et al., 2010, 2011). The reason for the conservation seems to be an evolutionary requirement of CCM3 to bind multiple partners. Indeed, this site is important for binding CCM2 (Li et al., 2010), the striatins (Kean et al., 2011), and paxillin (Li et al., 2011). In paxillin, the CCM3 FAT-H binds to short helical consensus sequences termed LD motifs (named for the first two residues of the sequence; Li et al., 2011). CCM3 also binds an LD-like motif within the striatin family of proteins (Kean et al., 2011), but how CCM2 and CCM3 interact has not been well described. Sequence alignments of CCM2 with both paxillin and striatin family LD and LD-like motifs revealed a putative CCM2 LD–like motif (Kean et al., 2011), located between the N-terminal phosphotyrosine-binding (PTB) domain (Liquori et al., 2003; Fisher et al., 2015) and the C-terminal harmonin homology domain (HHD; Fisher et al., 2013), but this has not been investigated further.

Here, we provide the first detailed mapping of the CCM3 binding site within CCM2, determine a 2.8-Å cocrystal structure of CCM3 with a CCM2 LD–like motif peptide that defines the CCM2–CCM3 interaction, and validate this interaction by point mutagenesis of CCM2 and CCM3. We establish the biological relevance of the interaction using knockdown and re-expression in endothelial cells. We reveal that CCM2–CCM3 interactions stabilize CCM2 and CCM3 protein levels by inhibiting their proteasomal degradation, and that crystallographically defined mutations that interrupt the CCM2–CCM3 interaction fail to rescue protein levels. We also show that the interaction between CCM2 and CCM3 is required for normal endothelial cell network formation. We have discovered a role for CCM3 that is independent of its recruitment to CCM2, where CCM3 expression in the absence of CCM2 is sufficient to support normal cell growth in culture. We provide a more complete molecular level description of CCM complex formation and its role in endothelial cells.

Results

CCM3 binds an interdomain region in CCM2

To understand the functional significance of the CCM2–CCM3 interaction, we first sought a detailed characterization of the CCM2–CCM3 interface. CCM2 contains an N-terminal PTB domain (Liquori et al., 2003; Fisher et al., 2015), followed by a linker region and an HHD (Fisher et al., 2013; Fig. 1 A), but the portion of CCM2 that binds to CCM3 has not previously been mapped. To probe the minimal region of CCM2 that could bind CCM3, we therefore conducted pull-down assays using various N-terminally tagged GST fusion constructs of CCM2 bound to glutathione Sepharose beads and purified, soluble N-terminally 6×His-tagged full-length CCM3. Bound CCM3 was detected by immunoblotting. We tested a nearly full-length protein (residues 1–438; $CCM2^{FL}$), a PTB domain construct (residues 51–251) that includes a significant portion of the linker region between the PTB and HHD domains ($CCM2^{PTB\text{-}LongLinker}$, $CCM2^{PTB\text{-}LL}$), a PTB domain construct (residues 51–238) that includes a shorter portion of the linker region ($CCM2^{PTB\text{-}ShortLinker}$, $CCM2^{PTB\text{-}SL}$), and a PTB domain construct (residues 51–223) predicted not to include residues of the interdomain linker ($CCM2^{PTB}$; Fig. 1 A). We found that CCM3 bound to $CCM2^{FL}$, $CCM2^{PTB\text{-}LL}$, and $CCM2^{PTB\text{-}SL}$, but displayed notably reduced binding to the PTB domain–alone construct, $CCM2^{PTB}$ (Fig. 1 B). Quantification revealed that $CCM2^{PTB}$ bound significantly lower amounts of CCM3 than the longer CCM2 constructs do (Fig. 1 C). Both $CCM2^{PTB\text{-}LL}$ and $CCM2^{PTB\text{-}SL}$ bound comparable levels of CCM3 ($P = 0.478$), while $CCM2^{FL}$ consistently bound slightly more CCM3 than $CCM2^{PTB\text{-}LL}$ ($P = 0.01$) or $CCM2^{PTB\text{-}SL}$ ($P = 0.004$). These data suggest that residues 223–238, located within the N-terminal portion of the linker between the PTB and HHD domains and containing a putative LD-like motif (Fig. 1 D), are necessary for the CCM2 interaction with CCM3.

To test whether the LD-like motif of CCM2 is sufficient to support CCM3 binding, we generated an N-terminally tagged GST fusion construct encoding residues 224–239 ($CCM2^{LD}$) and showed that this could efficiently pull down CCM3 (Fig. 1 E). We next compared $CCM2^{FL}$ and $CCM2^{LD}$ in pull-down experiments using increasing concentrations of purified 6×His-CCM3 and calculated apparent affinity constants for CCM3 binding. As shown in Fig. 1 F and Fig. 1 G, CCM3 bound both $CCM2^{FL}$ and $CCM2^{LD}$ in a dose-dependent saturable manner and produced affinity constants of 8.8 ± 1.6 µM and 8.6 ± 2.2 µM for $CCM2^{FL}$ and $CCM2^{LD}$, respectively (Fig. 1, F and G). Assessment of binding between GST-CCM2-LD immobilized on anti-GST biosensors and increasing concentrations of CCM3 by biolayer interferometry (Pall Life Sciences) revealed a similar affinity of 9.5 ± 2.5 µM (Fig. S1 A). These data show that the LD-like motif of CCM2 is necessary and sufficient to mediate the CCM3–CCM2 interaction and that the isolated LD-like motif binds with an affinity that is similar to that of the full-length CCM2. Furthermore, these affinities fall into the range of other FAT or FAT-H domain interactions with LD motifs (Table S1; Alam et al., 2014).

Cocrystal structure of CCM3 in complex with CCM2 LD-like motif

Based on our pull-down mapping experiments, we synthesized a 16-residue CCM2 peptide, S^{224}TIDFLDRAIFDGAST, and soaked pregrown CCM3 crystals with this peptide. We collected x-ray diffraction data at the National Synchrotron Light Source (NSLS) beamline X25, and obtained a 2.8-Å dataset ($\langle I \rangle / \langle \sigma(I) \rangle$ is 3.1 at 3.02 Å; Table S2). Structure determination by molecular replacement yielded a clear solution, and refinement was conducted to convergence for CCM3 alone. Once the refinement for CCM3 had converged, we were able to unambiguously build a single copy of the CCM2 peptide into a region of contiguous

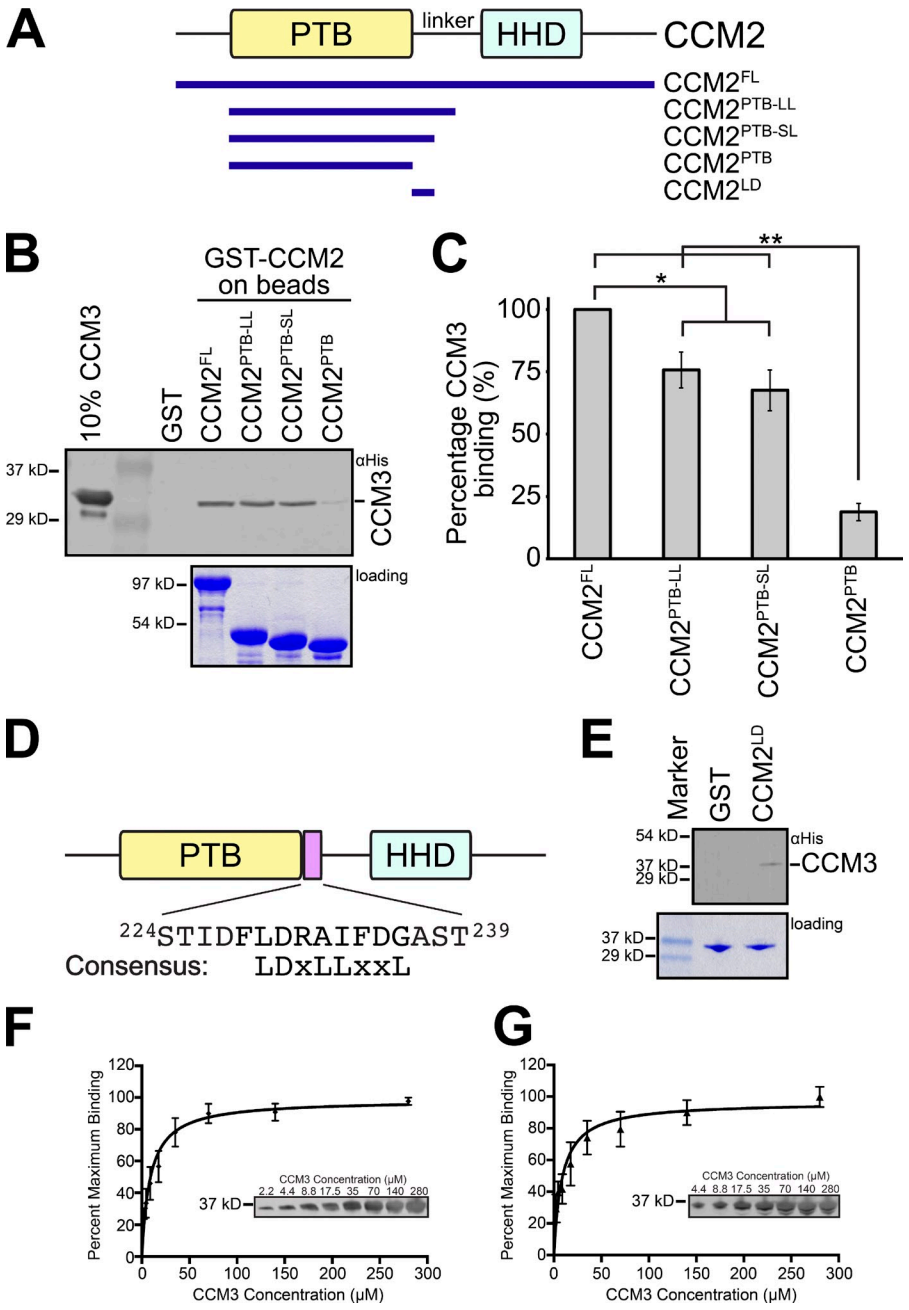

Figure 1. **Mapping of the CCM3–CCM2 interaction.** (A) Domain diagram for CCM2 and constructs used in this study. (B) Pull-down of 6×His-CCM3 by GST fusion CCM2 constructs. Pull-down was probed by immunoblotting for the His tag. (C) Quantification of pull-downs shown as a percentage of CCM3 that binds to $CCM2^{FL}$. Values represent mean ± SEM (error bars). $n = 5$. Unpaired t test: *, $P < 0.05$; **, $P < 0.001$. (D) CCM2 contains an LD-like motif C-terminal to its PTB domain. The LD-like motif is indicated and the sequence is shown. Consensus LD motif residues are shown. (E) 6×His-CCM3 can be pulled down by GST-$CCM2^{LD}$. Pull-down was probed by immunoblotting for the His tag. (F) Binding curve for CCM3 interaction with full-length CCM2. Increasing concentrations of 6×His-tagged CCM3 were incubated with a fixed concentration of GST-tagged $CCM2^{FL}$ on beads. The inset shows a Western blot. $n = 3$. (G) Same as in F, but GST-$CCM2^{LD}$ was used. $n = 3$. Error bars indicate SEM.

positive difference density located at the FAT-H domain HP1 site of one of the four CCM3 molecules in the asymmetric unit. We completed refinement for the CCM3–CCM2 complex and found that we could clearly build all residues of the CCM2 peptide into electron density. Overall, CCM3 is found in a highly similar conformation to that observed in previous structures; it is a two-domain protein with an N-terminal dimerization domain and a C-terminal FAT-H domain (Fig. 2 A). Good electron density is observed for the bound CCM2 peptide (Fig. 2, B and C; and Fig. S1 B).

CCM2 LD–like motif binds to the HP1 pocket of CCM3

The LD-like motif of CCM2 binds the CCM3 HP1 site, which is juxtaposed between the αG and αH helices of the CCM3 FAT-H domain. The CCM2 LD–like motif forms a 3 and 1/2 turn α-helix that is parallel to CCM3 helix αG (Fig. 2 D), with its N terminus pointing toward the closed end of the FAT-H domain. It buries a surface area of 557 $Å^2$ from CCM3 and 709 $Å^2$ from CCM2 to yield a total buried surface area of 1,266 $Å^2$ (PISA server; Krissinel and Henrick, 2007). The CCM2 LD–like α-helix presents a broadly hydrophobic surface comprising residues T225, I226, F228, L229, A232, I233, G236, and A237 to the HP1 site of CCM3 (Fig. 2 E). This hydrophobic stripe is composed of residues different from those previously proposed to form the interface (Kean et al., 2011). CCM3 residues I131, I134, A135, I138, L142, V168, F174, L178, and aliphatic parts of S171, K132, and K139 form the bulk of the hydrophobic surface to which the CCM2 LD–like motif binds (Fig. 2 F). Hydrogen bonds are formed between CCM2 residue D230 and both S175

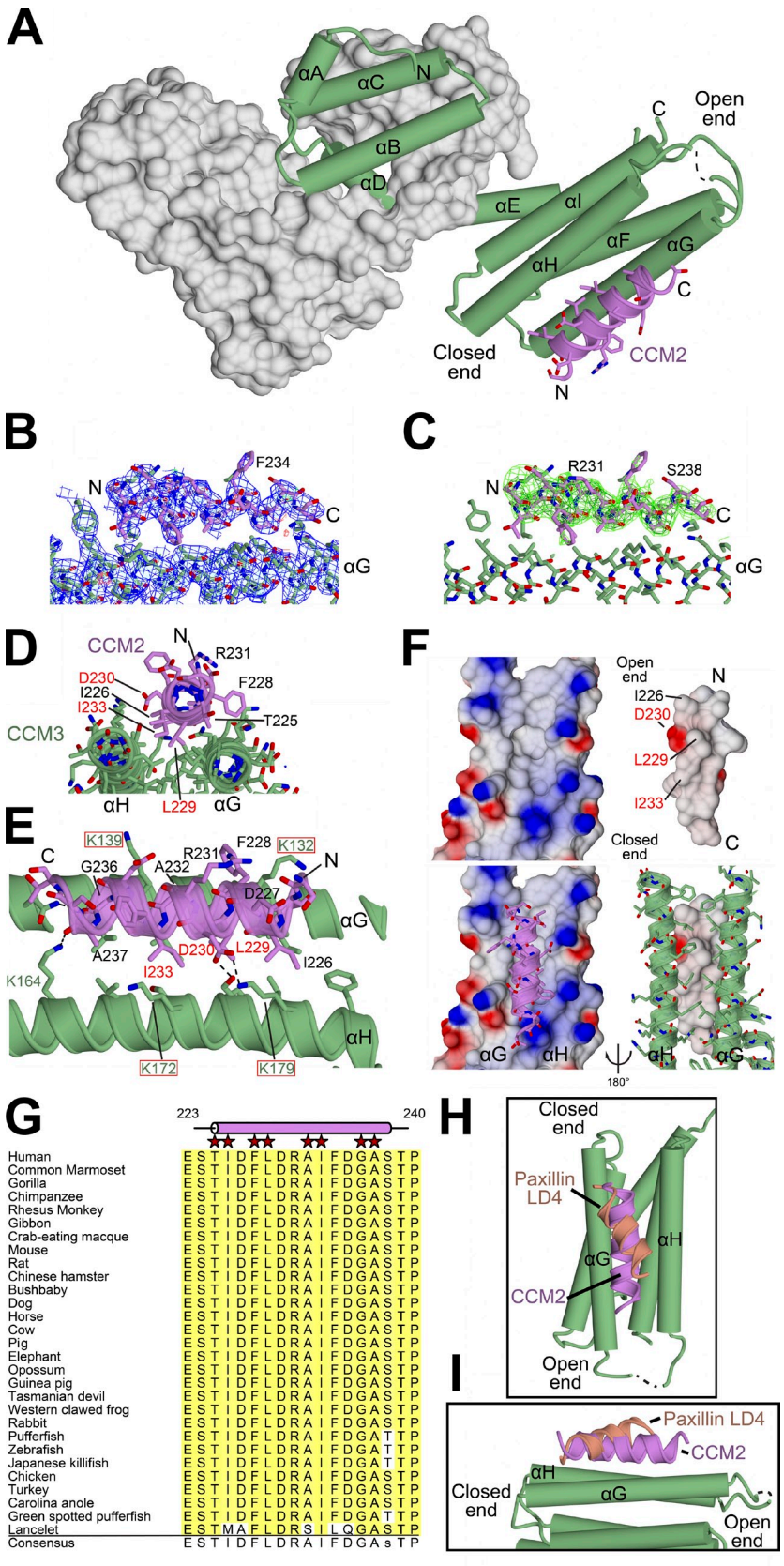

Figure 2. **Cocrystal structure of CCM3 with CCM2 LD–like motif.** (A) One molecule of the CCM3 dimer is shown in surface representation (gray) and the other as a cartoon (green). CCM3 helices are shown as labeled cylinders. The open and closed ends of the FAT-H domain are indicated. CCM2 peptide is shown as a cartoon (purple), with the side chains shown as sticks. The N and C termini are indicated. The broken line indicates a chain break in the maps. (B) Final refined electron density for the CCM2 LD–like motif peptide bound to CCM3. The $2F_{obs}$-F_{calc} map is shown in dark and light blue for +1σ and +2σ, respectively. The F_{obs}-F_{calc} map is shown in green and red for +3σ and −3σ, respectively. (C) Unbiased difference density for the CCM2 LD–like peptide. The F_{obs}-F_{calc} map is shown in dark and light green for +3σ and +2σ, respectively. The model was refined to convergence without the peptide, resulting in a very clear difference map that allowed unambiguous model building. (D and E) Structure of CCM3 in complex with CCM2 LD–like motif shown in cartoon and stick format. Residues mutated in this study are labeled in red for CCM2 and boxed in red for CCM3. The broken line indicates a hydrogen bond. (F) Electrostatic potential of CCM3 (left) and CCM2 (right) in open book format. Bottom panels show the same view with either CCM2 (purple) or CCM3 (green) shown in cartoon format. (G) Sequence alignment of the CCM2 LD–like motif. Residue numbers correspond to the human protein, and the CCM3-interacting residues are indicated by stars. (H and I) CCM2 binds to CCM3 in a conformation that is distinct from previously observed FAT or FAT-H domain interactions with LD motifs. Shown is the superposition of CCM3 (green) in complex with CCM2 LD–like motif (pink) and CCM3 in complex with paxillin LD4 motif (salmon; PDB no. 3RQG). CCM3 is not shown for the paxillin-bound structure, but superposes extremely well. The broken lines indicate chain breaks.

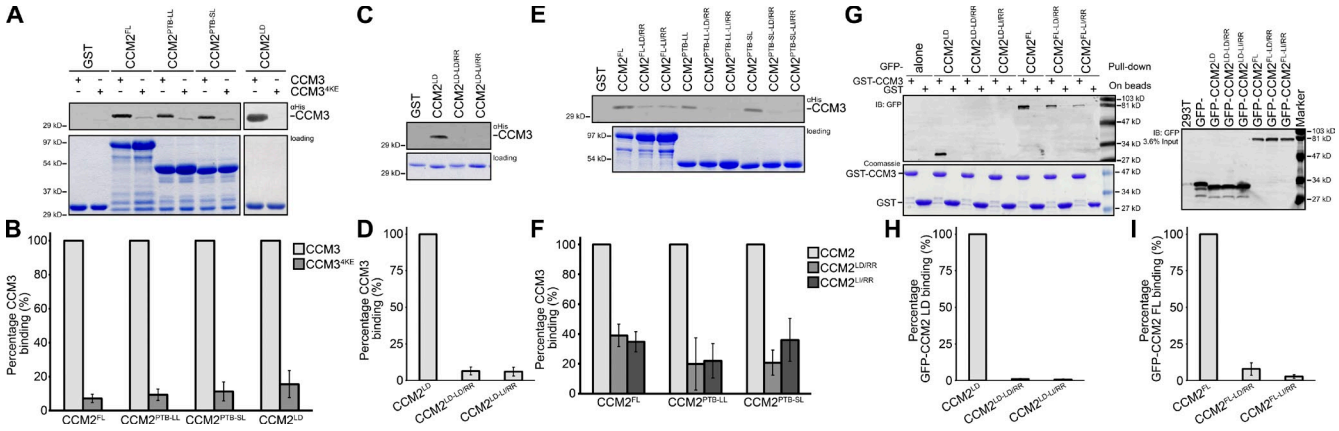

Figure 3. **Biochemical analysis of the interaction between CCM3 and CCM2.** (A and B) Pull-down of 6×His-CCM3 or 6×His-CCM3^{4KE} by GST fusion CCM2 constructs. Pull-down was probed by immunoblotting (A) and quantified (mean ± SEM, error bars; n = 3) as a percentage of CCM3 that binds to each CCM2 construct (B). (C and D) Pull-down of 6×His-CCM3 by mutated GST-CCM2^{LD}. Pull-down was probed by immunoblotting (C) and quantified (mean ± SEM, error bars; n = 4) as a percentage of CCM3 that binds to wild-type CCM2^{LD} construct (D). (E and F) Pull-down of 6×His-CCM3 by mutated GST fusion CCM2 constructs. Pull-down was probed by Western blotting (E) and quantified (mean ± SEM, error bars; n = 4) as a percentage of CCM3 that binds to each wild-type CCM2 construct (F). (G) Pull-down of heterologously expressed GFP-CCM2 by purified GST-CCM3. GFP-fusions of either full-length CCM2 or the CCM2 LD–like motif expressed in HEK 293T cells were pulled down by either GST or GST-CCM3 immobilized on beads. 3.6% input is shown. (H) Quantification of pull-downs of CCM2 LD–like motif constructs shown in G (mean ± SEM, error bars; n = 3) as a percentage of GFP-CCM2^{LD} that binds to GST-CCM3. (I) Quantification of pull-downs of full-length CCM2 constructs shown in G (mean ± SEM, error bars; n = 3) as a percentage of GFP-CCM2^{FL} that binds to GST-CCM3.

and K179 from CCM3. Additional hydrogen bonds are formed between the backbone carbonyl of CCM2 residue G236 and the side-chain amino group of CCM3 residue N146, as well as between the backbone carbonyl of CCM2 residue A237 and CCM3 residue K164 (Fig. 2 E). These interactions seem to form a capping box to account for the δ-helix dipole of the CCM2 peptide. All CCM3 residues mentioned above are completely conserved over evolution (33 species; Li et al., 2010), with the exception of N146, which is serine in the human body louse. Likewise, each of the CCM2 residues that mediate the interaction with CCM3 are completely conserved over evolution (Fig. 2 G).

Comparison of CCM3-CCM2 interactions with CCM3-paxillin interactions

Comparison of our CCM3–CCM2 crystal structure with the previously determined cocrystal structures of CCM3 in complex with the LD motifs of paxillin (Li et al., 2011) revealed several differences. The CCM2 LD–like motif binds CCM3 by a larger surface area (1,266 Å^2 buried compared with 880–998 Å^2), is a longer α-helix (3 and 1/2 turns compared with 2–3 turns), and is substantially more parallel to helix αG than the observed interactions of CCM3 with the paxillin LD motifs (Fig. 2, H and I). The CCM2 LD–like motif is also substantially more parallel to helix αG than observed interactions of paxillin LD motifs with FAK or Pyk2 FAT domains (Hoellerer et al., 2003; Lulo et al., 2009; Li et al., 2011; Alam et al., 2014). At the amino acid interaction level, CCM2 does not contain the spatially conserved ELD or DLE tripeptide motif interactions that are characteristic of the CCM3–paxillin complexes (Li et al., 2011). Instead, CCM2 residue F228 occupies the spatial location of the tripeptide glutamic acid. The CCM2–CCM3 interaction is therefore conformationally divergent from previously characterized LD motif interactions with FAT or FAT-H domain proteins.

Mutational analysis of the CCM2-CCM3 interaction

To validate the crystallographically observed interfaces, we introduced point mutations that we expected would interrupt the interactions between CCM3 and CCM2. We then probed the impact of these mutations using our pull-down assay followed by Western blot analysis. We began by generating a quadruple lysine–to–glutamic acid mutation in the FAT-H domain of CCM3 (K132E, K139E, K172E, K179E), termed CCM3^{4KE} (Fig. S1, C and D). We previously showed that charge reversal for these four exquisitely conserved lysines interrupts CCM3 interactions with both paxillin (Li et al., 2011) and CCM2 (Li et al., 2010). To confirm this using the current system, we compared CCM3 and CCM3^{4KE} binding to GST fusions of CCM2^{FL}-, CCM2^{PTB-LL}-, CCM2^{PTB-SL}-, or CCM2^{LD}-bound to beads. We found that in all cases the amount of CCM3^{4KE} binding to beads approximated to background, clearly indicating that mutants of these conserved lysines interrupt CCM3's interaction with CCM2 (Fig. 3, A and B).

Analysis of our CCM2–CCM3 cocrystal structure further suggested that two CCM2 double mutations, L229R/D230R and L229R/I233R, might disrupt the hydrophobic interface between CCM3 and the CCM2 LD–like motif. We therefore first introduced these mutations into the GST-CCM2^{LD} construct (CCM2$^{LD-LD/RR}$, CCM2$^{LD-LI/RR}$) and conducted pull-down analysis using purified CCM3. We found that both CCM2$^{LD-LD/RR}$ and CCM2$^{LD-LI/RR}$ were unable to pull down CCM3 (Fig. 3, C and D). We next introduced the same double mutations into the CCM2^{FL}, CCM2^{PTB-LL}, and CCM2^{PTB-SL} constructs (CCM2$^{FL-LD/RR}$, CCM2$^{FL-LI/RR}$, CCM2$^{PTB-LL-LD/RR}$, CCM2$^{PTB-LL-LI/RR}$, CCM2$^{PTB-SL-LD/RR}$, CCM2$^{PTB-SL-LI/RR}$). Again, each of these doubly mutated CCM2 constructs were severely impaired in their ability to pull down CCM3 (Fig. 3, E and F). Finally, to confirm that similar results are obtained when proteins are expressed in mammalian cells, we generated GFP-tagged expression constructs

for wild-type and mutant CCM2 and assessed their binding to purified recombinant GST-tagged CCM3. Consistent with results using purified proteins, CCM3 bound to full-length GFP-CCM2 and to GFP-CCM2^{LD}, but not to GFP-CCM2 or GFP-CCM2^{LD} mutants (Fig. 3, G, H, and I). Collectively, our mutagenic studies confirm the crystallographically determined CCM2–CCM3 interface.

Reciprocal protein stabilization through CCM2-CCM3 interaction

Our in vitro structural and biochemical studies reveal how CCM2 and CCM3 interact and provide powerful tools to investigate the functional significance of the interaction. While CCM2 and CCM3 have each been implicated in a variety of signaling pathways, the roles that CCM2–CCM3 interactions play in their function remained unknown. To test whether complex formation is important for protein stabilization, we first used lentiviral delivery of shRNA expression constructs to knock down CCM2 or CCM3 in the widely used human umbilical vein endothelial cell-derived line EA.hy926. EA.hy926 cells retain many endothelial features but lack the high degree of donor and isolation-driven variability seen in primary endothelial cells, and, importantly, they can be stably cultured, permitting us to perform knockdown and rescue studies (Bouïs et al., 2001). Using two independent shRNA constructs for each gene, we showed for the first time that knockdown of CCM2 leads to reduction in the levels of CCM3 (Fig. 4 A). Likewise, CCM3 knockdown reduces CCM2 protein levels (Fig. 4 A). Quantification of multiple independent experiments (Fig. 4 B) revealed that, depending on the knockdown constructs used, an 81–93% knockdown of CCM2 led to a 31–35% reduction of CCM3 protein levels, whereas an 85–92% knockdown of CCM3 led to a 44–48% decrease in CCM2. The effects of loss of CCM2 or CCM3 on expression levels of their binding partners was not due to inhibition of transcription, as quantitative real-time PCR (qPCR) indicated that CCM2 knockdown actually increased CCM3 message levels and that, likewise, CCM3 knockdown increased CCM2 message levels (Fig. S2 A). These data suggest that knockdown of CCM2 or CCM3 may reduce the stability of CCM3 or CCM2 protein. Consistent with this idea, 8 h of treatment with the proteasome inhibitor MG132 restored CCM3 expression in CCM2 knockdown cells without altering CCM2 levels and restored CCM2 levels in CCM3 knockdown cells without altering CCM3 levels (Fig. 4, C, D, and E).

Our results suggest that formation of the CCM2–CCM3 complex may protect its components from proteasomal degradation. To test this further, we reexpressed full-length GFP-CCM2 or GFP-CCM3 in the respective CCM knockdown cells and assessed the consequences on partner protein expression levels. Results are shown for shRNA constructs producing the greatest knockdown (shCCM2$^{\#1}$ and shCCM3$^{\#2}$), but qualitatively similar data were obtained using the other shRNA constructs (unpublished data). Immunoblotting demonstrated that the reexpressed GFP-tagged protein was overexpressed compared with endogenous CCM2 or CCM3 levels (Fig. 4 F). Nonetheless, as shown in Fig. 4 F and quantified in Fig. 4 H, expressing GFP-CCM2 in CCM2 knockdown cells restored endogenous CCM3 expression levels to wild-type levels, while overexpressing GFP-CCM2 in scramble shRNA control cells had no impact on CCM3 levels. Expression of GFP alone had no impact on CCM2 levels in control or CCM2 knockdown cells (Fig. 4, F and G). Importantly, GFP-CCM2 requires an intact CCM3-binding site to increase CCM3 expression in CCM2 knockdown cells, as CCM2 with LD-like motif mutation L229R/I233R, GFP-CCM2$^{LI/RR}$, did not restore endogenous CCM3 expression (Fig. 4, F and H). Similarly, in CCM3 knockdown cells, expression of GFP-CCM3, but not GFP alone or GFP-CCM3^{4KE}, rescued endogenous CCM2 expression (Fig. 4, F and G). The inability of GFP-CCM2$^{LI/RR}$ to rescue endogenous CCM3 expression, or of GFP-CCM3^{4KE} to rescue endogenous CCM2 expression, is not due to a failure of mutant protein expression, as immunoblotting (Fig. 4 F) and fluorescence microscopy (not depicted) show it to be well expressed. Surprisingly, expression of GFP-CCM3, or to a lesser extent GFP-CCM3^{4KE}, in control cells inhibited expression of endogenous CCM3 (Fig. 4, F and H). qPCR suggests that this is at least partly due to a reduction in endogenous CCM3 mRNA (Fig. S2 B). However, competition between GFP-CCM3 and endogenous CCM3 for binding to endogenous CCM2 may contribute to the lower levels of endogenous CCM3 in the GFP-CCM3 compared with GFP-CCM3^{4KE}–expressing cells, as the proteasome inhibitor MG132 partially restores endogenous CCM3 levels in GFP-CCM3–expressing cells (Fig. S2 C).

In summary, coupling our identification of CCM2 and CCM3 mutants that disrupt their binding with analysis of knockdown cells reexpressing wild-type and mutant proteins strongly suggests that the CCM2–CCM3 interaction is important for maintenance of CCM2 and CCM3 protein levels.

CCM3 expression controls cell number

When generating the CCM2 and CCM3 knockdown cells used in Fig. 4, we observed that knockdown cultures expanded more slowly than parental EA.hy926 cells or control shRNA–expressing cells. Careful assessment over 5 d of culture clearly established that knockdown of CCM2 or CCM3 strongly impaired the increase in cell number (Fig. 5 A). This effect was evident for both knockdown constructs of each gene and appeared to be strongest with the more efficient knockdown constructs. Re-expression of wild-type but not mutant CCM2 or CCM3 restored cell numbers in CCM2 and CCM3 knockdown cells, respectively (Fig. 5 B). These data suggested that a CCM2–CCM3 complex is important for regulating cell number, either through effects on cell proliferation or on cell survival. However, whether formation of a CCM2–CCM3 complex directly contributes to the process, or is important only because it stabilizes protein expression, was not clear. We therefore performed additional GFP-CCM expression experiments in knockdown cells. Although CCM2–CCM3 complex formation is clearly normally important in regulating protein levels, partner binding is not absolutely essential for protein expression because overexpressed binding-defective GFP-CCM mutants can be detected (Fig. 4 F). We therefore expressed GFP-CCM2 in CCM3 knockdown cells and assessed cell numbers. CCM3 knockdown cells have very little CCM3 and exhibit reduced levels of CCM2. Reconstitution with GFP-CCM2 increased

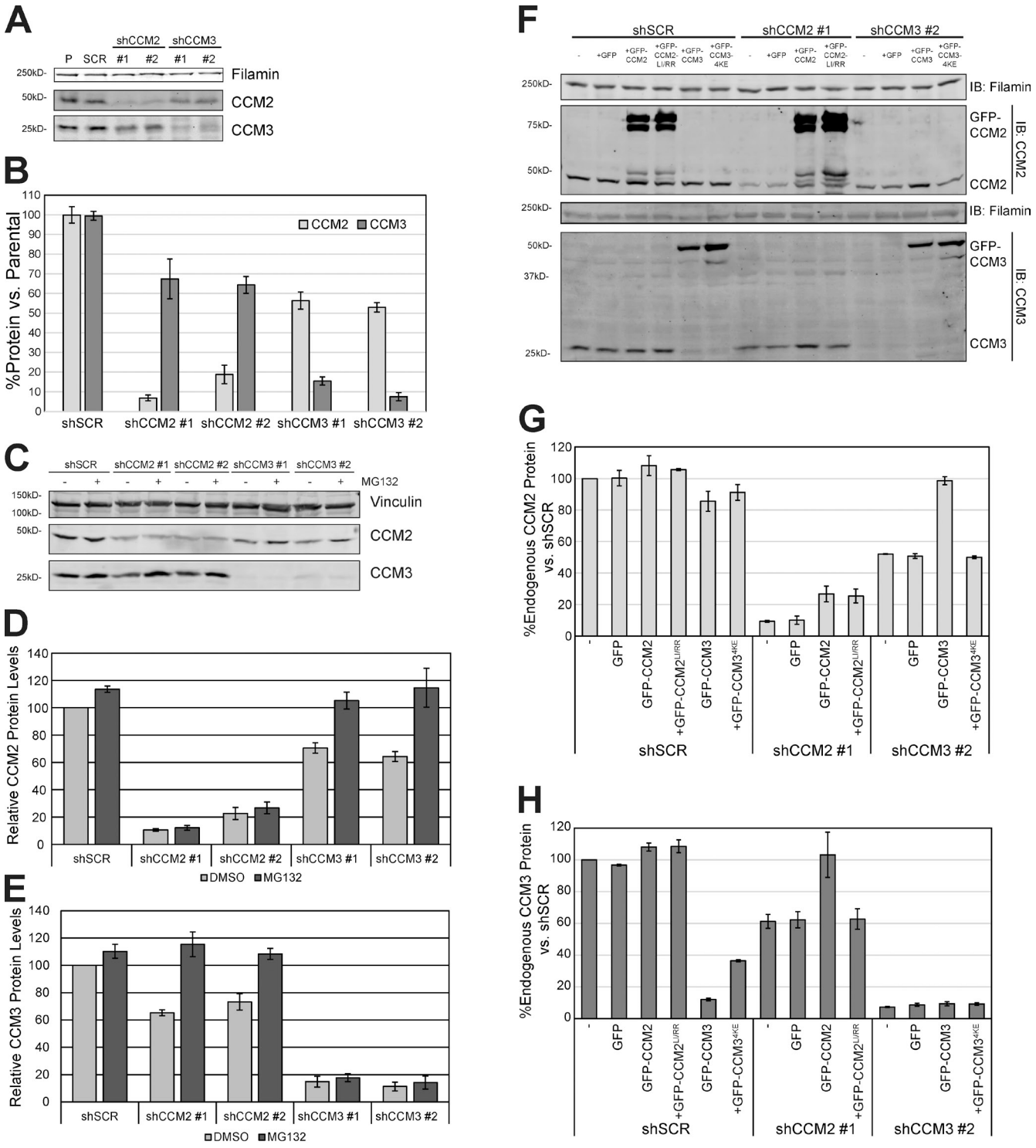

Figure 4. **Reciprocal protein stabilization through CCM2–CCM3 interaction.** (A and B) EA.hy926 cells stably infected with control scrambled shRNA (shSCR) or with shRNAs against CCM2 (shCCM2 #1 and #2) or CCM3 (shCCM3 #1 and #2) were lysed, and CCM2 and CCM3 expression was probed by immunoblotting (A). (B) Immunoblots were quantified using Image Studio and normalized for the filamin A loading control (mean ± SEM, error bars; $n = 5$). (C–E) Proteasome inhibition in CCM2 or CCM3 knockdown cells. (C) Stable shSCR, shCCM2 #1, shCCM2 #2, shCCM3 #1, and shCCM3 #2 knockdown lines were treated with proteasome inhibitor MG132 for 8 h, cells were lysed, and CCM2 and CCM3 expression was probed by immunoblotting. (D and E) CCM2 (D) and CCM3 (E) immunoblots were quantified using Image Studio (mean ± SEM, error bars; $n = 3$). (F–H) CCM2 or CCM3 reexpression in knockdown cells. Stable shSCR, shCCM2 #1, and shCCM3 #2 knockdown lines were infected with lentivirus expressing GFP, GFP-CCM2, GFP-CCM2$^{LI/RR}$ (deficient for CCM3 binding), GFP-CCM3, or GFP-CCM3^{4KE} (deficient for CCM2 binding) as indicated. (F) After selection, cells were lysed and CCM2, CCM3, and filamin A (loading control) were detected by immunoblotting. CCM2 (G) and CCM3 (H) immunoblots were quantified using Image Studio (mean ± SEM, error bars; $n = 3$).

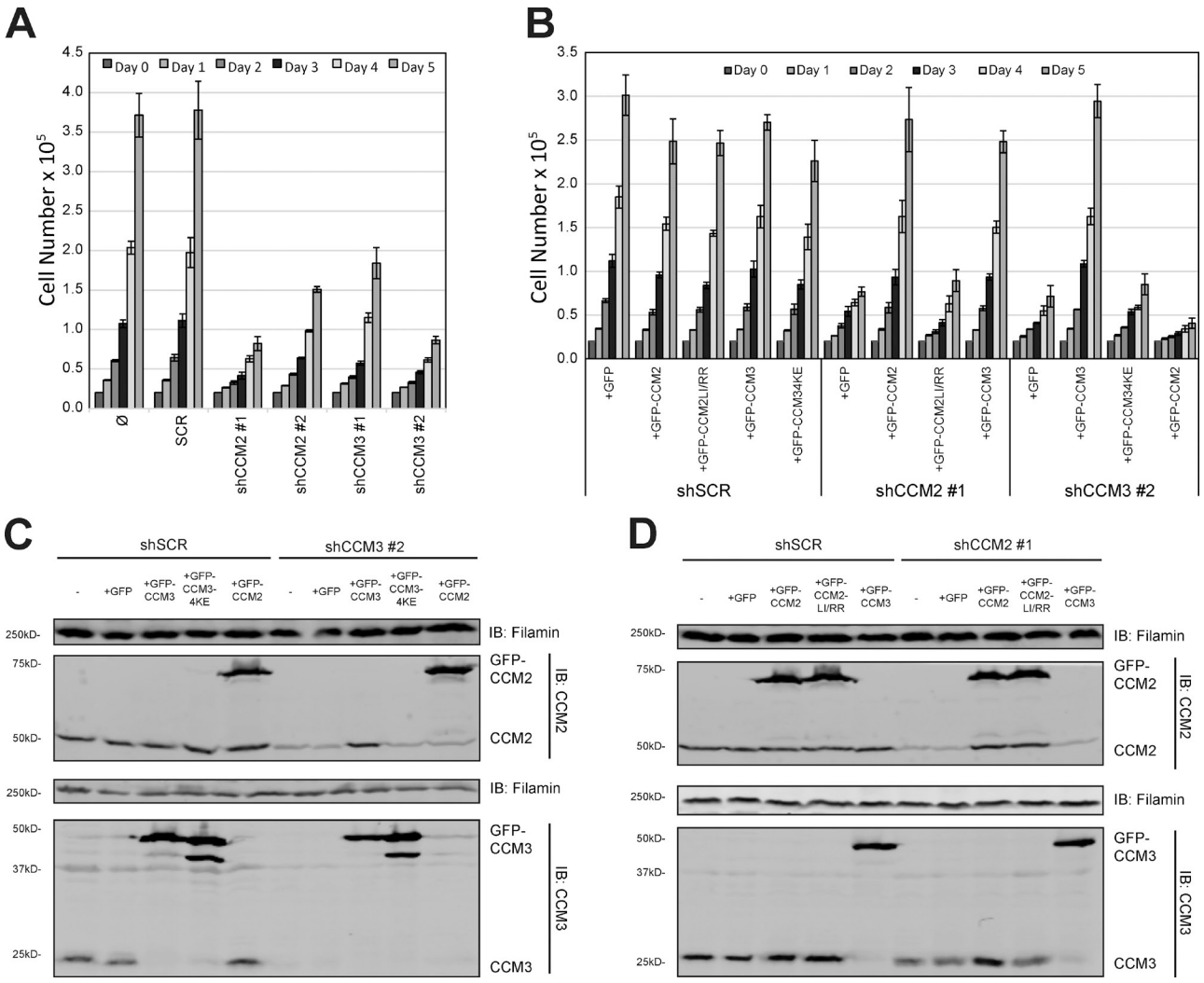

Figure 5. **CCM3 is required for cell growth.** (A) Stable CCM2 or CCM3 knockdown cells were evaluated for 5 d in a cell growth assay and compared with uninfected/parental cells (∅) and cells infected with a virus expressing a scrambled hairpin (shSCR). Bar graphs represents the mean cell number ± SEM (error bars) from at least nine experiments. (B) The effects of expressing GFP, or wild-type or mutant GFP-CCM2 and GFP-CCM3 in shSCR, shCCM2 #1, or shCCM3 #2 EA.hy926 cells were evaluated in a 5-d cell growth assay. Bar graphs represent the mean cell number ± SEM (error bars) from at least nine experiments. (C and D) Immunoblotting was used to verify the expression of the exogenous and endogenous CCM2 and CCM3 proteins in CCM2 knockdown (C) and CCM3 knockdown (D) cells.

total CCM2 levels without rescuing endogenous CCM3 levels (Fig. 5 C) but failed to increase cell growth (Fig. 5 B). Indeed, overexpressing CCM2 in the absence of CCM3 further reduced cell numbers below those seen in CCM3 knockdown cells (Fig. 5 B). Thus, CCM2 expression in the absence of CCM3 was not sufficient to permit normal expansion of cell number. However, when we overexpressed GFP-CCM3 in CCM2 knockdown cells, it was sufficient to largely rescue the cell number phenotype (Fig. 5 B), without rescuing the expression of endogenous CCM2 (Fig. 5 D). Consistent with the inability of GFP-CCM3^{4KE} to rescue defects in CCM3 knockdown cells (Fig. 5 B), expressing GFP-CCM3^{4KE} also failed to rescue cell numbers in CCM2 knockdown cells (Fig. S3 A). These data clearly implicate CCM3 in the control of cell numbers. Expression of GFP-CCM2$^{LI/RR}$ in CCM2 knockdown cells is presumably unable to rescue cell numbers because it cannot restore CCM3 expression levels (Fig. 4 F). We suggest that the inability of GFP-CCM3^{4KE} to restore growth of CCM3 knockdown cells is not due to its inability to bind and stabilize CCM2, but instead is because it disrupts CCM3 binding to other partner proteins, such as striatin or paxillin (Kean et al., 2011; Li et al., 2011). Consistent with this suggestion, paxillin knockdown EA.hy926 cells exhibit growth inhibition comparable to that seen in CCM3 knockdown cells, whereas striatin 1 knockdown cells show an even more profound growth defect (Fig. S3, B and C). CCM3 expression is not required to maintain paxillin or striatin expression levels, and CCM3 levels are normal in paxillin and striatin knockdown cells (Fig. S3, B and D). Future work will address the question of whether the CCM3–paxillin and CCM3–striatin interactions contribute to their effects on cell number. Nonetheless, we conclude that loss of CCM3 results in cell proliferation defects and that, even in the absence of CCM2, forced CCM3 expression restores cell numbers.

Both CCM2 and CCM3 are required for normal endothelial network formation

Loss of CCM proteins has previously been shown to impair the ability of endothelial cells to assemble into vessel-like tubular networks resembling capillaries in vitro (Borikova et al., 2010; Wüstehube et al., 2010). We therefore used our knockdown and reconstitution system to investigate the importance of the CCM2–CCM3 interaction in this process. In keeping with previous reports (Jones et al., 1998), stimulating confluent EA.hy926 cell cultures with 2.5% ethanol for 3 h followed by plating on growth factor–reduced Matrigel in low serum (0.5% FBS) medium for 20 h resulted in the assembly of cells into branched networks. The short time course, coupled with the use of low serum and growth factor–reduced Matrigel, means there is little to no cell proliferation during the assay, minimizing the potential effect of altered growth rates on tube formation. As expected, both parental and scramble control knockdown EA.hy926 cells formed striking networks (Fig. 6 A). In addition to inspection of networks, we quantified the percentage of cells in networks (defined as linear or branched assemblies of at least five cells) across multiple fields and at least three independent experiments (see Materials and methods for details). This revealed that >90% of parental and control cells were in networks (Fig. 6 B). Consistent with previous work (Borikova et al., 2010), knockdown of CCM2 or CCM3 severely perturbed network formation, resulting in very few cells (<20%) being present in networks, and the very few networks present were generally very short (Fig. 6, A and B).

We next assessed the impact of expressing wild-type or mutant GFP-CCM2 or GFP-CCM3 in these knockdown cells. Scramble control cells retained their ability to form networks on expression of GFP or GFP fusion wild-type or mutant CCMs (Fig. 6 C). However, despite retaining most cells within networks (Fig. 6 F), the organization of networks formed by cells expressing GFP-CCM3^{4KE} was clearly perturbed (Fig. 6 C). To assess the quality of the network, we counted the number of nodes (branch points) and ends per field, and normalized them to the total number of cells (see Materials and methods for details). This revealed that, consistent with an interconnected branched network, control cells expressing GFP, wild-type, or mutant GFP-CCM2, or GFP-CCM3, exhibited more nodes than ends (Fig. 6 G). However, control cells expressing GFP-CCM3^{4KE} had significantly fewer ($P < 0.005$) nodes and greatly increased ends, reflecting the fragmented nature of the network. We hypothesize that the defect in network formation is due to the partial loss of endogenous CCM3 in the GFP-CCM3^{4KE}-expressing shSCR cells (Fig. 4 F).

In CCM3 knockdown cells, GFP-CCM3 expression, which also restores endogenous CCM2 levels (Fig. 4, E and F), largely rescued network formation, although visual inspection indicates that the networks were not quite as robust as those observed in control cells (Fig. 6, C and D). Quantification showed that GFP-CCM3 reexpression restored the percentage of cells in networks and the number of nodes, but these networks had increased numbers of ends (Fig. 6, F and G), which reflects more breaks in the network. However, expression of GFP or GFP-CCM3^{4KE} in CCM3 knockdown cells completely failed to rescue networks, the number of cells in networks, or the number of nodes (Fig. 6, D, F, and G). Expression of GFP-CCM2 in the CCM3 knockdown cells partially rescued the percentage of cells in networks (Fig. 6 F) but the segments that formed were short, with little branching (Fig. 6 D). The profound defect in the ability of these cells to form normal networks is reflected in the low number of nodes and the high number of ends (Fig. 6 G), which is consistent with the induction of short unbranched segments. These data show that normal levels of fully functional CCM3 are required for network formation, and attempts to bypass this requirement by only restoring CCM2 expression produce only very weak rescue.

As expected, GFP-CCM2 expression restored network formation in CCM2 knockdown cells (Fig. 6 E), although again the networks appeared less robust than those in control cells with increased ends, despite having a normal percentage of cells in networks and normal node numbers (Fig. 6, F and G). Interestingly, as was the case for GFP-CCM2 expression in shCCM3 cells, GFP-CCM3 expression in CCM2 knockdown cells produced a partial rescue of the percentage of cells in networks (Fig. 6 F) but only supported formation of relatively short networks with reduced complexity, fewer nodes, and increased ends compared with GFP-CCM2–rescued networks (Fig. 6 G). Thus, although CCM2 and CCM3 apparently each have independent roles in network formation, complete rescue requires the restoration of expression of both proteins. When we attempted to rescue CCM2 knockdown cells with GFP-CCM2$^{LI/RR}$, we observed that, similar to the weak rescue of CCM3 knockdown cells with GFP-CCM2 (Fig. 6, D and F), there was an increase in the percentage of cells in networks (Fig. 6 F) and a small increase in the number of nodes compared with GFP alone ($P < 0.01$; Fig. 6 G), but a large increase in the number of ends (Fig. 6 G). However, the networks formed were more variable than observed in any other conditions, with many fields showing essentially no rescue, others short poorly branched cell clusters, and some showing more extensive/complex networks (Fig. 6 E and Fig. S4). We do not believe that this is due to variation in GFP-CCM2$^{LI/RR}$ expression because the reexpressing populations were relatively homogenous when assessed by flow cytometry (unpublished data). However, autofluorescence from the Matrigel-coated plates makes it difficult to directly assess GFP levels in the networks. In conclusion, our data suggest that although CCM2 and CCM3 have some independent roles in network formation, both proteins are required for optimum network formation. We further show that a CCM2 LD–like motif–CCM3 FAT-H domain interaction is important for CCM2 and CCM3 protein stabilization and hence for endothelial cell network formation.

Discussion

Human genetic studies have revealed that haploinsufficiency of *KRIT1*, *CCM2*, or *CCM3* predisposes the individual to CCM disease, and genetic studies in mice and zebrafish have implicated these proteins in cardiovascular development (Draheim et al., 2014). Notably, CCM2 has been shown to interact with both KRIT1 and CCM3, which suggests that a heterotrimeric CCM complex contributes to CCM (Draheim et al., 2014; Fisher and Boggon, 2014). However, detailed characterization of the complex

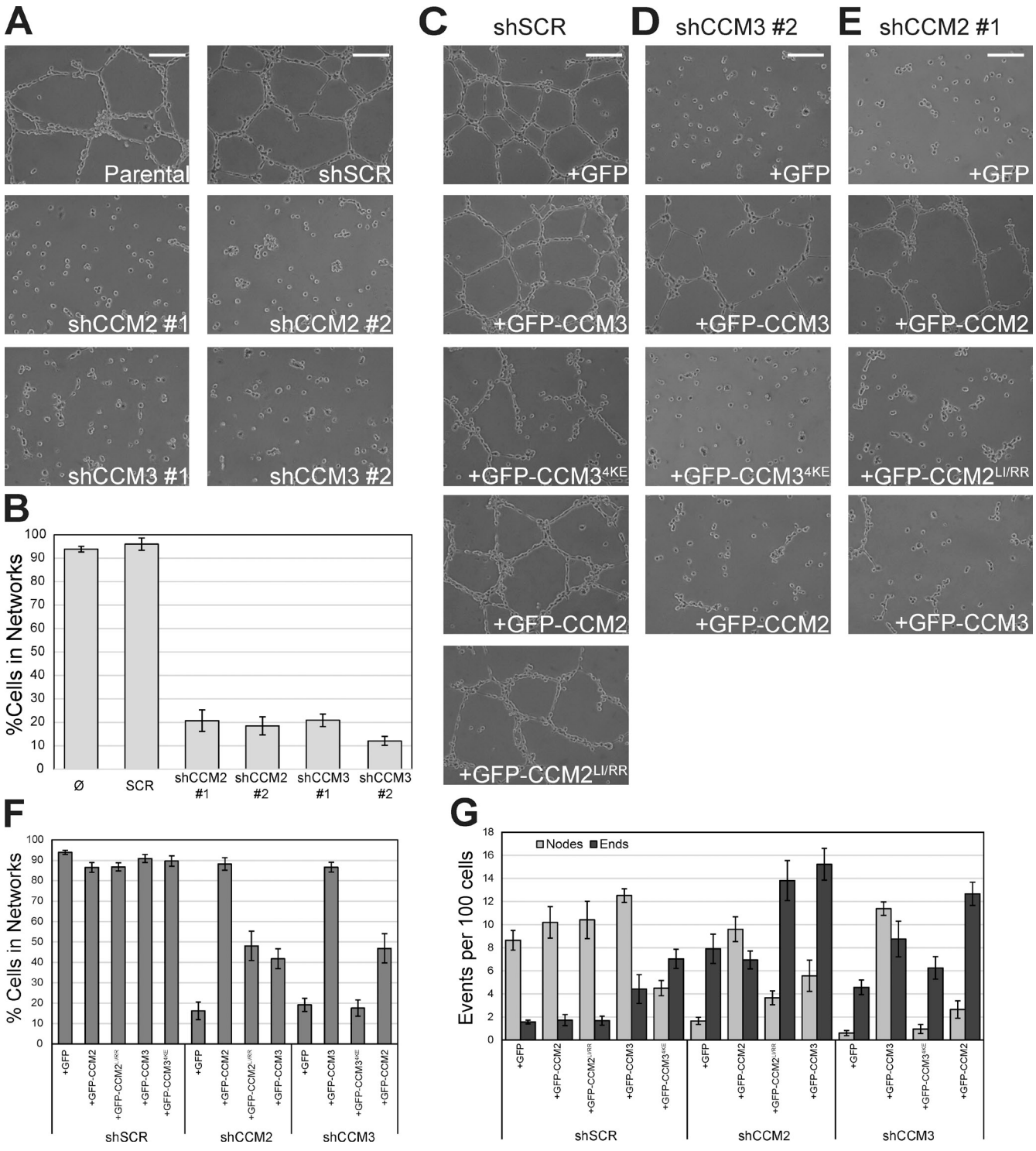

Figure 6. **The CCM2–CCM3 interaction contributes to endothelial cell network formation.** (A) Representative images of networks formed by parental, control knockdowns, and CCM2 or CCM3 knockdown EA.hy926 lines. Bars, 100 µm. (B) Quantification of the mean ± SEM (error bars) percentage of cells within a network from four independent experiments. At least six fields were quantified per experiment. (C–E) Representative images of networks from stable control (C), CCM3 (D), or CCM2 (E) knockdown lines overexpressing GFP or wild-type or mutant GFP-CCM proteins. (F and G) Quantification of networks in C–E from three independent experiments with at least six fields quantified per experiment. The mean (±SEM, error bars) percentage of cells within a network (F) and mean (±SEM, error bars) number of network nodes and ends per 100 cells in the field are shown.

has proven elusive, hindering its functional analysis. Disease-causing mutations, knockout phenotypes, and knockdown studies in cultured cells show CCM2 and CCM3 to be essential for a range of activities including regulation of vascular cell polarity, endothelial permeability, and cytoskeletal organization (Draheim et al., 2014). Here we have characterized the CCM2–CCM3 interaction and provided the first analysis of its functional significance, identifying CCM complex–dependent and –independent processes.

CCM2 and CCM3 interact with a variant of canonical FAT-LD motif binding

In this study, we provide the first definitive description of the interaction between CCM3 and CCM2. We report a comprehensive mapping, crystallographic analysis, and biochemical mutagenesis validation of the interaction, as well as measurement of the CCM3–CCM2 binding affinity. Although multiple studies have investigated the structural biology of the CCM proteins (Fisher and Boggon, 2014), here we provide the first view of CCM complex formation at the molecular level. We observe that the CCM2–CCM3 interaction represents an unusual mode of FAT or FAT-H domain–binding to LD motifs. The CCM2 peptide is almost parallel to helix αG. This is unusual, as most LD motif interactions with FAT domains seem to occur with a more significant angle between the helices. Indeed, we have previously determined the crystal structures of CCM3 with the LD motifs of paxillin and found that these interactions are not parallel to CCM3 helix αG, a finding that was also observed for FAK and Pyk2 interactions with paxillin (Li et al., 2010). To test whether the CCM2 LD–like motif might also interact with the FAK FAT domain, we conducted pull-down assays using purified FAK FAT domain and $CCM2^{LD}$, but did not observe an interaction (unpublished data). Therefore, the interactions of CCM2 LD–like motif seem to be specific for CCM3 over other FAT domain proteins. We also tested the affinity of the interaction and found it to be in the range previously observed for FAT domain protein interactions with LD motifs. The structural studies therefore provide a rational basis for our functional analyses.

The CCM2 and CCM3 interaction is required for protein stability

Although prior studies have implicated other CCM protein interactions in the stabilization of protein expression (Faurobert et al., 2013), here we present the first evidence that the CCM2–CCM3 interaction stabilizes protein levels. We further show that, as was reported for KRIT1–ICAP1 protein stabilization (Faurobert et al., 2013), the ability of CCM2 and CCM3 to form a complex appears to protect them from proteasomal degradation. The loss of CCM3 after knockdown of CCM2, or of CCM2 after CCM3 knockdown, is not due to reduced mRNA levels for the nontargeted gene. Indeed, it is noteworthy that despite the decrease in protein the message levels increase, perhaps as part of an adaptive response attempting to restore protein levels. Similar results were observed for the KRIT1–ICAP1 complex (Faurobert et al., 2013). Furthermore, we find that CCM3 overexpression leads to a reduction in endogenous CCM3 message. These results are consistent with the idea that CCM protein levels are tightly controlled both through complex-regulated proteasomal degradation and through an uncharacterized regulation of transcription or mRNA stability.

A notable difference between the KRIT1–ICAP1 studies (Faurobert et al., 2013) and our CCM2–CCM3 findings is the extent of protein level decrease after the loss of the binding partner. Although loss of CCM2 leads to a decrease in CCM3 and vice versa, the percentage of the binding partner lost is more modest than that seen with KRIT1–ICAP1, where a complete loss of ICAP1 leads to a complete loss of KRIT1 (Faurobert et al., 2013). This could be a reflection of the relative amount of protein found in this interaction because only the CCM2 and CCM3 that are in complex with one another would be impacted by this effect. CCM2 and CCM3 each have several other binding partners (Draheim et al., 2014; Fisher and Boggon, 2014), and while CCM3 levels are not substantially reduced after paxillin or striatin knockdown, and vice versa, other CCM3 partners such as the germinal center kinase III family potentially protect CCM3 from degradation (Fidalgo et al., 2012). We also note that exogenous overexpression of CCM2 or CCM3 in the absence of their binding partner is possible, showing that formation of a CCM2–CCM3 complex is not absolutely essential for protein expression. However, we hypothesize that in this case it is the high level of production of the exogenous protein that permits accumulation even in the face of proteasomal degradation. Nonetheless, in light of our data showing codependence for normal expression levels, it is now necessary to reevaluate studies that characterized the functional consequences of loss of CCM2 or CCM3 to determine the specific roles of CCM2 and CCM3.

Roles of CCM3 outside of the CCM complex

Loss of any one of the CCM genes causes similar disease phenotypes. However, patients with mutations in CCM3 (the most ancient of the three CCM proteins) are often more severely affected (Riant et al., 2013). Additionally, mass spectrometry has indicated that while KRIT1 and CCM2 form an abundant complex that binds to CCM3 in substoichiometric amounts, a large proportion of CCM3 is also associated with the STRIPAK complex (Goudreault et al., 2009). Collectively, this suggests that CCM3 has CCM complex–independent functions. Our data indicate that regulation of cell proliferation or survival may be one of these functions. Although loss of either CCM2 or CCM3 inhibits cell growth, overexpression of CCM3 can rescue this phenotype in the absence of CCM2, indicating that the CCM2–CCM3 interaction is not required for the maintenance of cell growth. It is therefore likely that CCM2-deficient cells are defective in cell growth because CCM3 levels are diminished; indeed, reexpression of $CCM2^{LI/RR}$, which cannot restore CCM3 levels, fails to rescue cell numbers. If true, a CCM3 mutation that specifically interrupts CCM2 binding, but not CCM3 binding, to other partners should rescue this phenotype. Unfortunately this is not currently possible because the CCM3 FAT-H HP1 site is used to bind multiple partners. However, the inability of the $CCM3^{4KE}$ mutant to rescue growth of CCM2-deficient cells does suggest that the interaction of another binding partner at that site is required to maintain proliferation. Consistent with this, we find that knockdown of paxillin or striatin 1 also impairs cell growth. Although further studies will be required to test whether the CCM3–striatin or CCM3–paxillin interactions contribute to this effect, CCM3-mediated targeting of GCKIII kinases to striatin may be a candidate mechanism linking the proliferation-associated phenotype of the GCKIIIs (Gordon et al., 2011; Sugden et al., 2013) and cell cycle regulation of striatin (Kemp and Sprague, 2003).

Roles of CCM2 and CCM3 within the CCM complex

Although it has been shown that the loss of any of the CCM proteins leads to a defect in endothelial tube formation (Borikova et al., 2010), those studies do not take into account the dependence of the CCM2–CCM3 interaction for protein stability. By expressing CCM2 in CCM3 knockdown lines or CCM3 in CCM2 knockdown lines, we demonstrate that endothelial cells lacking only CCM2 or CCM3 retain a residual ability to form networks. These data suggest that both CCM2 and CCM3 have roles outside of the fully formed tripartite CCM complex that contribute to network formation. Interestingly, the CCM2 mutant defective in binding CCM3 ($CCM2^{LI/RR}$) partially rescued the shCCM2 line, which further indicates essential roles for CCM2 outside of binding and stabilizing CCM3, presumably at least in part through its interaction with KRIT1. However, characterization of the networks clearly shows that they are severely impaired, with shorter, less branched sections than in controls, and as $CCM2^{LI/RR}$ did not rescue as completely as wild-type CCM2, there is clearly a dependence on the CCM2–CCM3 interaction for network formation. There are at least two possible explanations for this observation: either CCM2 and CCM3 signal together in a complex, or their interaction is required for the stabilization of CCM3 protein levels, and it is the decrease of CCM3 that prevents complete rescue. Exactly why CCM depletion decreases network formation remains an important question but the known roles for CCM proteins in establishing cell polarity, stabilizing cell–cell contacts, and regulating the cytoskeleton and cellular contractility are likely to be involved (Draheim et al., 2014)

Implications for understanding the CCM complex and the functions of CCM2 and CCM3 in CCM disease

The loss of either CCM2 or CCM3 is associated with ∼35% of familial CCM cases, although the clinical presentation of CCM3 loss is more severe. As these proteins directly interact with one another and have overlapping, but distinct, roles, it was important to begin to dissect which are the common roles for CCM2 and CCM3 that drive the similarities in their phenotypes, and which are their distinct functions. Our structure-guided study shows that the CCM2–CCM3 interaction is required for reciprocal stabilization, and that this interaction is important for endothelial network formation. Our study also alludes to a CCM3-specific role in endothelial cell growth. Therefore, the more severe clinical presentation (earlier onset age, smaller percentage of patients with asymptomatic lesions, increased incidence of cerebral hemorrhage of CCM3 loss) may be associated with the impacts of CCM3 on proliferative or survival pathways.

Materials and methods

Protein preparation

N-terminally hexa-histidine (6×His)-tagged human full-length CCM3 was expressed and purified as described previously (Li et al., 2010). In brief, human CCM3 (Uniprot ID Q9BUI8) was subcloned into a modified pET-32 vector (T7 promoter; EMD Millipore) with an N-terminal polyhistidine tag and produced in *Escherichia coli* by induction with 0.2 M IPTG. After lysate clarification, the supernatant was applied to a HisTrap (GE Healthcare) affinity column and eluted with 400 mM imidazole, the tag was removed by TEV protease, and the resultant protein was further purified using Mono S ion exchange chromatography. Human CCM2 (Uniprot ID Q9BSQ5) constructs encoding residues 1–438, 51–251, 51–238, and 51–223 were subcloned into a modified pET-32 vector (T7 promoter) with a GST N-terminal tag cleavable by TEV protease and expressed in *E. coli* by induction with 0.2 M IPTG at 16°C. GST-CCM2-LD–like motif (residues 224–239) was generated by insertion of synthetic oligonucleotides into pGEX-6p-1 (tac promoter; GE Healthcare) using QuikChange mutagenesis (Agilent Technologies). Point mutations in CCM2 and CCM3 were induced by QuikChange mutagenesis and mutant proteins were prepared or purified like the corresponding wild-type proteins. GST-tagged proteins were purified on glutathione Sepharose 4B beads and eluted with reduced glutathione. Further purification was by size exclusion chromatography on a Superdex 200 (GE Healthcare) column.

GST-pull down, Western blot assays, and gel quantification

GST-CCM2 proteins and their mutants were bound to 20 µl of glutathione Sepharose 4B beads (GE) and incubated with 10 µg of purified 6×His-CCM3 protein in pull-down buffer (50 mM Tris, pH 7.5, 150 mM NaCl, 0.1% Triton X-100, and protease inhibitor cocktail [Roche]) at 4°C for 1 h with shaking. After centrifugation at 13,000 rpm for 1 min, the supernatant was removed and the beads were washed three times with pull-down buffer. The beads were then analyzed by SDS-PAGE and transferred to a nitrocellulose membrane for probing with mouse anti-His (H-1029; Sigma-Aldrich) and anti–mouse IR Dye800 antibodies (LI-COR Biosciences). Equal amounts of GST fusion protein on the beads were verified by Coomassie staining. The Western blot results were scanned and validated with an infrared imaging system (Odyssey CLx; LI-COR Biosciences). Gel quantification was performed using ImageJ software (Girish and Vijayalakshmi, 2004). For quantification, background intensity was subtracted. For binding affinity calculation, quantifications were normalized to background GST binding and each band was divided by the B_{max} value of that assay. The separate datasets were then imported to Prism 6 (GraphPad Software) for final curve fitting. Binding affinity calculation used one-site saturation binding curve fitting and was performed using Prism 6 software. Each pull-down and Western blot assay was performed more than three times and showed consistent results. Unpaired *t* tests were performed using Prism 6.

Biolayer interferometry

The biolayer interferometry technique was used to measure binding kinetics with a BLItz instrument (Pall Life Sciences). Anti-GST biosensors were incubated in binding buffer (20 mM Hepes, pH 7.4, 0.3 mM EDTA, and 150 mM NaCl) before GST fusion protein association measurements by incubation against 4 µl of 50 µg/ml purified GST fusion CCM2 LD–like motif. Probes were then incubated for 5 min against purified CCM3 at concentrations varying between 2.6 and 173 µM. Control experiments using GST alone were performed in identical conditions, and R equilibrium was calculated using the BLItz software package. Multiple repeats were conducted at each concentration of CCM3, with 27 data points, allowing binding affinity calculation by one-site saturation binding curve fitting concentration of added CCM3 to R equilibrium obtained from the BLItz software package. Results were analyzed using Prism 6. Concentrations of proteins were measured by UV using a NanoDrop spectrophotometer (GE Healthcare), and experiments were performed at room temperature.

Crystallization and peptide soaking

Purified CCM3 was concentrated to 10 mg/ml. Cocrystallization of CCM3 and CCM2 LD–like peptide failed, so we conducted a soaking experiment. Crystallization of CCM3 alone was conducted at room temperature using the hanging-drop vapor diffusion method and precipitant conditions ranging between 0.1 and 0.2 M potassium fluoride and 15–20% PEG-3350. The CCM2 LD–like motif–derived peptide used for crystal soaking was synthesized (Tufts University Core Facility) with N-terminal acetylation and C-terminal amidation modifications and corresponds to the following sequence of human CCM2: (224–239) N′-STIDFLDRAIFDGAST-C′. The peptide was dissolved in 40 mM Tris-Cl, pH 8.0, to a concentration of 6 mM. For peptide soaking, unliganded CCM3 crystals were transferred from the original drop to a new drop containing 1.0–2.0 mM peptide and increased precipitant concentration (0.1–0.2 M potassium fluoride, 25–35% PEG-3350), then allowed to soak for several hours to overnight. CCM3 crystals in complex with CCM2 LD–like motif peptide were cryoprotected in 25% glycerol.

Data collection and structure determination

Data for the CCM3–CCM2 cocrystals were collected at NSLS Beamline X25 at a wavelength of 1.100 Å. The cocrystals diffracted to 2.8 Å, and the data were processed using the HKL2000 package (Otwinowski and Minor, 1997). The structure was determined by molecular replacement using PHASER (McCoy et al., 2007) in the CCP4 package (Collaborative Computational Project, Number 4, 1994). The native orthorhombic CCM3 crystal structure (Protein Data Bank [PDB] accession no. 3L8I) containing four chains in one asymmetric unit was used as the search model. This yielded a solution with translation z scores of 47.0 and four CCM3 chains forming two dimers in one asymmetric unit. Model building and refinement followed using the programs COOT (Emsley and Cowtan, 2004), REFMAC5 (Murshudov et al., 2011), and Phenix (Adams et al., 2010). The first round of model refinement after molecular replacement using sequentially rigid-body refinement, TLS refinement, and restrained-refinement in REFMAC5 yielded R/R_{free} values of 22.5%/31.2%. After ~15 rounds of refinement, the R/R_{free} values converged to 24.5%/29.8%. For the four CCM3 chains, clear unattributed unambiguous electron density was observed adjacent only to CCM3 chain C. The lack of buildable density observed adjacent to chains A, B, and D can be explained by poor density for the FAT-H domain found in chain A, high *B*-factors for chain B (density is visible for the CCM2 peptide but unbuildable; the average *B*-factor for the chain B FAT-H domain is 81.2 $Å^2$ compared with 61.3 $Å^2$ for chain C), and clashes with crystal symmetry mates for chain D. COOT was used to place a 16-residue helix in this density, and unambiguously determined its directionality. Some crystal contacts are observed at the C terminus of the peptide, but manual modeling of the reverse orientation suggests that both orientations would be compatible with these contacts. Furthermore, the fit of the interaction between CCM3 and CCM2 is clearly more complementary for the built structure than for the modeled reverse orientation. These analyses support the unambiguous direction of the CCM2 peptide observed in the density. We conducted standard model building and refinement, and the final model was validated using MolProbity (Davis et al., 2004). The final complex of CCM3 with a CCM2 LD–like motif was deposited in the PDB under accession code 4TVQ. Structural figures were generated using CCP4mg (McNicholas et al., 2011). CCM2 LD–like motif sequence alignment over 29 species was generated using ClustalW and Aline (Bond and Schüttelkopf, 2009).

Pull-down of heterologously expressed CCM2 by purified GST-CCM3

GST-tagged CCM3 and GST alone were purified by affinity chromatography using glutathione Sepharose 4B beads followed by gel filtration using a size exclusion chromatography column (Superdex 200; GE Healthcare). GFP-tagged CCM2 LD–like motif (peptide sequence STIDFLDRAIFDGAST) and GFP-tagged full-length CCM2 expression constructs were generated in the pGFP-C1 vector (CMV promoter) and transfected into HEK 293T cells using Lipofectamine. Expression of GFP-CCM2 constructs was verified by Western blotting. GST or GST-CCM3 were incubated with glutathione Sepharose 4B beads for 1 h. GFP-CCM2–expressing cells were lysed using PBST buffer (1× PBS with 1% Triton X-100 plus cocktail protease inhibitors), and the supernatants were incubated with GST- or GST-CCM3–coated beads for 2 h. After washing the beads with PBST buffer three times, samples were analyzed by Western blotting using mouse anti-GFP (sc-9996; Santa Cruz Biotechnology, Inc.) and Dye800 anti–mouse antibodies (827-08364; LI-COR Biosciences). Western blots were developed using an infrared imaging system (Odyssey; LI-COR Biosciences). Quantification was performed using Image Studio Lite software. All signals were normalized with coated GST proteins and the expression level of GFP-tagged proteins.

Lentiviral knockdown and overexpression

Lentiviral constructs in the pLKO vector (U6 promoter) containing shRNAs (target sequences in brackets or parentheses) against CCM2 (TRCN0000083233 [#1, GCCCAGGTCCTCTACTGTG] and TRCN0000083237 [#2, GCTGAGCGACTATATTGAG]), CCM3 (TRCN0000141584 [#1, CCAGGATGTTGAATGGGAT] and TRCN0000144821 [#2, GAATGGGATTATTGCCATCTT]), paxillin (TRCN0000123134-36 [#1, CCCGACCTAATTGTCTTTGTT; #2, CCTGACGAAAGAGAAGCCT; #3, CCCAACTGGAAACCACACA]), TRCN0000293920 (#4, GGCCATCCTGGAGAACTATAT), TRCN0000286555 (#5, ACCCAACTGGAAACCACACAT), TRCN0000286485 (#6, GCCTTACTGTCAGAACTGCTT), and striatin 1 (TRCN0000036944-48 [#1, GCCTGAGCGAATACAAGTT; #2, GCGGTGAAGATCGAGATAC; #3, CCCACCTAGAAGCTGTTAC; #4, CGTCATTGATACTTCAACAAT; #5, GCAAGGGATATACAAGCAT]) along with a scrambled control (TRC library-based lentiviral scramble; catalog no. SHC002) were obtained from a TRC shRNA library (Sigma-Aldrich). Wild-type and mutant human CCM2 and CCM3 cDNAs were subcloned into pEGFP-C1 driven by the CMV promoter (Takara Bio Inc.) and were authenticated by DNA sequencing. Lentiviral CCM2 and CCM3 expression constructs were generated by following the protocol described in Fu et al. (2008). In brief, attL1/attL2 sites were added to GFP-tagged cDNA by two rounds of PCR, and the final product was run on a 0.7% agarose gel and purified by gel extraction. The second round PCR products were used in a Gateway cloning reaction (Life Technologies) to insert the GFP-tagged construct into CMV-pLENTI-Hygro (Addgene). The LR reaction was transformed into Max Efficiency STBL2 competent cells (Invitrogen) and confirmed by sequencing.

Lentiviruses were produced by cotransfecting packaging vectors psPAX2 (viral proteins Gag and Rev under the SV40 promoter; Addgene plasmid #12260, a gift from D. Trono, École Polytechnique Fédérale de Lausanne, Lausanne, Switzerland) and pMD2.G (viral protein VSV-G expressed under the CMV promoter; Addgene plasmid #12259, a gift from D. Trono) into HEK 293T cells with the shRNA construct. Viral supernatant was collected 48 and 72 h after transfection and filtered with a 0.45-µm filter.

Generation and analysis of stable cell lines

To establish polyclonal knockdown or overexpression lines, EAhy926 cells (cultured in DMEM containing 10% FBS, 1% sodium pyruvate, 1% penicillin/streptomycin, and 2% HAT supplement; Gibco) were incubated with the viral supernatant and 8 µg/ml polybrene for 18 h, and infected cells were selected with 2 µg/ml Puromycin (pLKO) or 50 µg/ml Hygromycin (CMV-pLENTI-Hygro) as was appropriate. Knockdown was assessed by immunoblotting of stable lines lysed in RIPA buffer (50 mm Tris, pH 8.0, 150 mm NaCl, 1% Triton X-100, 0.5% sodium deoxycholate, and 0.1% SDS) containing protease inhibitor mixture tablets (Roche). Immunoblotting was performed with fluorescent secondary antibodies (IR Dye800 or IR Dye680; LI-COR Biosciences) and scanned on the Odyssey CLx infrared imaging system. Quantification was performed on the raw images in Image Studio (LI-COR Biosciences); lanes were defined and bands were automatically identified. The profile feature was used to identify band boundaries and lane background was subtracted. The signal for the protein of interest was normalized to that of the loading control. Optimization of images for publication was performed by adjusting the brightness and contrast in Image Studio (LI-COR Biosciences).

Proteasome inhibition studies

Stable EAhy.926 cell lines were incubated with either DMSO or 10 µM proteasome inhibitor MG132 (Sigma-Aldrich) for 8–16 h as indicated. Cells were lysed in RIPA buffer, protein concentration was measured with a BCA assay (Pierce; Life Sciences), and lysates were fractionated by SDS-PAGE and analyzed by immunoblotting.

Antibodies

Anti-CCM2 (SAB1400724; Sigma-Aldrich), anti-striatin (610838; BD), anti-paxillin (610051; BD), anti-vinculin (V9131; Sigma-Aldrich), and anti-GFP (Rockland Immunochemicals) antibodies were purchased. The rabbit polyclonal anti–filamin A antibody raised against purified recombinant human filamin A residues 2045–2329, produced in *E. coli*, has been described previously (Kiema et al., 2006), and the rabbit polyclonal anti-CCM3 antibody (antigen was purified full-length human CCM3 recombinantly produced from *E. coli*) was a gift from W. Min (Yale University, New Haven, CT; Li et al., 2010).

Cell growth assays

EA.hy926 cells were plated in 12-well tissue culture plates (2×10^4 cells/well). Every 24 h for 5 d, three wells for each cell line were trypsinized, stained with Trypan blue, and counted using a TC20 automated cell counter (Bio-Rad Laboratories) according to the manufacturer's guidelines.

Endothelial network formation

Network formation in the EA.hy926 cell line was assayed as described in Jones et al. (1998). Cells were grown in 60-mm tissue culture dishes until confluent, and growth media was replaced with complete media containing 2.5% ethanol for 3 h. The wells of 12-well tissue culture plates were evenly coated with growth factor–reduced Matrigel (0.25 ml/well) and the Matrigel was allowed to solidify at 37°C for 30 min. Ethanol-stimulated cells were trypsinized, counted, and resuspended at 4×10^4 cells/ml in DMEM containing 0.5% FCS. 2 ml of cell suspension was plated onto the Matrigel-coated well and incubated at 37°C. 16–20 h later, the media was removed and the wells were gently washed before adding 1 ml of DMEM

containing 0.5% FCS and 2.5 µM DRAQ5. Cells were incubated at 37°C for an additional 30 min, and phase and DRAQ5 images were taken using an inverted microscope (Eclipse Ti; Nikon) with a 20× objective, 0.45 NA objective lens and an EXi Blue camera (QImaging). Micro-Manager open source software was used in the acquisition of the images, which were adjusted for contrast and analyzed using ImageJ. Network formation was quantified by counting the number of connected cells in randomly selected fields and dividing by the total number of cells in the same field. To distinguish networks from cell clumps, a network was defined as containing a minimum of five cells connected in a linear or branched fashion such that a single segment has more cells along the length than the width. Networks were also assessed by counting the number of nodes (defined as the junction point of at least three segments) and ends (defined as the termination of segments) per field, and normalized per 100 cells in the field.

qPCR

Total RNA was extracted from cells using the RNeasy Plus kit (QIAGEN) according to the manufacturer's instructions. RNA (1 µg) was reverse transcribed using the iScript cDNA synthesis kit (Bio-Rad Laboratories). qPCR was performed with iTaq Universal SYBR Green Supermix (Bio-Rad Laboratories). 50-µl reactions were performed in triplicate for each sample on a thermal cycler (C-1000 Touch; Bio-Rad Laboratories). Melt curves were evaluated using CFX Manager (Bio-Rad Laboratories). Ct values were determined with the same software, and normalization was done with the house-keeping genes B2M and GAPDH, yielding very similar results. Expression levels of each target gene were calculated with *B2M* as a reference gene and compared with control. Primer sequences are as follows: CCM2 forward, CATCGACTTTCTGGACAGAG; and reverse, GTAGAAGAGTCATCGCTGTG; CCM3 forward, ATGATGTGGCCCTCTAAGG; and reverse, CACACTGATCTTAGGTATGACAC; GAPDH forward, AAGGAGAGCTCAAGATTTGG; and reverse, GGCAACAATATCCACTTTACC; B2M forward, GAGGCTATCCAGCGTACTC; and reverse, CCAGACACATAGCAATTCAGG.

Sequence alignment

Sequence alignment of the CCM2 LD–like motif over 29 species was generated using ClustalW and Aline (Bond and Schüttelkopf, 2009). The alignment consisted of CCM2 from: *Homo sapiens* (human), UniProt ID Q9BSQ5; *Callithrix jacchus* (common marmoset), F6RW31; *Gorilla gorilla gorilla* (gorilla), G3QEW3; *Pan troglodytes* (chimpanzee), H2QUJ0; *Macaca mulatta* (rhesus monkey), H9G0F8; *Nomascus leucogenys* (gibbon), G1QVN9; *Macaca fascicularis* (crab-eating macaque), G7P1T7; *Mus musculus* (mouse), Q8K2Y9; *Rattus norvegicus* (rat), B1H273; *Cricetulus griseus* (Chinese hamster), G3HMC4; *Otolemur garnettii* (bushbaby), H0WW12; *Canis lupus familiaris* (dog), F1Q1Q9; *Equus caballus* (horse), F6Z7I5; *Bos taurus* (cow), E1B8H2; *Sus scrofa* (pig), F1ST61; *Loxodonta africana* (elephant), G2U3F2; *Monodelphis domestica* (opossum), F7G883; *Cavia porcellus* (guinea pig), H0VFM0; *Sarcophilus harrisii* (Tasmanian devil), G3VYU4; *Xenopus tropicalis* (Western clawed frog), F6YW88; *Oryctolagus cuniculus* (rabbit), G1T9C9; *Takifugu rubripes* (pufferfish), H2SK83; *Danio rerio* (zebrafish), Q6DRP4; *Oryzias latipes* (Japanese killifish), H2MPA3; *Gallus gallus* (chicken), E1C144; *Meleagris gallopavo* (turkey), G1MVK6; *Anolis carolinensis* (Carolina anole), H9G940; *Tetraodon nigroviridis* (green spotted pufferfish), H3CEX3; and *Branchiostoma floridae* (lancelet), C3ZRW2.

Accession numbers

The final complex of CCM3 with CCM2 LD–like motif was deposited in the PDB under accession no. 4TVQ.

Online supplemental material

Fig. S1 documents biolayer interferometry for the CCM2–CCM3 interaction, as well as presenting a simulated annealing omit map of the crystal structure and size exclusion chromatography for CCM3. Fig. S2 shows qPCR for CCM2 and CCM3 levels and protein levels after proteasome inhibitor treatment. Fig. S3 shows that loss of CCM3 binding partners Striatin or Paxillin leads to defects in cell growth, but does not affect CCM3 expression. Fig. S4 shows variability in network formation in CCM2 knockdown cells rescued with GFP-CCM2$^{LI/RR}$. Table S1 documents the apparent binding affinities of FAT or FAT-H domains with LD motifs. Table S2 gives data collection and refinement statistics. Online supplemental material is available at http://www.jcb.org/cgi/content/full/jcb.201407129/DC1.

We wish to thank M. Allaire, H. Zhang, W. Min, S-E. Jordt, NSLS beamlines X25 and X6A, and Advanced Photon Source beamline NE-CAT.

This work was funded by grants from National Institutes of Health (R01NS085078 and T32GM007324) and by the American Cancer Society (to K.M. Draheim), the National Science Foundation (to O.S. Fisher), and the American Heart Association (X. Li).

The authors declare no competing financial interests.

Author contributions: X. Li, K.M. Draheim, D.A. Calderwood, and T.J. Boggon conceived and designed the experiments. X. Li, K.M. Draheim, R. Zhang, and O.S. Fisher generated reagents and performed the experiments. X. Li, K.M. Draheim, G. Villari, D.A. Calderwood, and T.J. Boggon analyzed the data. X. Li, K.M. Draheim, D.A. Calderwood, and T.J. Boggon wrote the paper.

Submitted: 28 July 2014
Accepted: 19 February 2015

References

Adams, P.D., P.V. Afonine, G. Bunkóczi, V.B. Chen, I.W. Davis, N. Echols, J.J. Headd, L.W. Hung, G.J. Kapral, R.W. Grosse-Kunstleve, et al. 2010. PHENIX: a comprehensive Python-based system for macromolecular structure solution. *Acta Crystallogr. D Biol. Crystallogr.* 66:213–221. http://dx.doi.org/10.1107/S0907444909052925

Alam, T., M. Alazmi, X. Gao, and S.T. Arold. 2014. How to find a leucine in a haystack? Structure, ligand recognition and regulation of leucine-aspartic acid (LD) motifs. *Biochem. J.* 460:317–329. http://dx.doi.org/10.1042/BJ20140298

Bond, C.S., and A.W. Schüttelkopf. 2009. ALINE: a WYSIWYG protein-sequence alignment editor for publication-quality alignments. *Acta Crystallogr. D Biol. Crystallogr.* 65:510–512. http://dx.doi.org/10.1107/S0907444909007835

Borikova, A.L., C.F. Dibble, N. Sciaky, C.M. Welch, A.N. Abell, S. Bencharit, and G.L. Johnson. 2010. Rho kinase inhibition rescues the endothelial cell cerebral cavernous malformation phenotype. *J. Biol. Chem.* 285:11760–11764. http://dx.doi.org/10.1074/jbc.C109.097220

Bouïs, D., G.A. Hospers, C. Meijer, G. Molema, and N.H. Mulder. 2001. Endothelium in vitro: a review of human vascular endothelial cell lines for blood vessel-related research. *Angiogenesis.* 4:91–102. http://dx.doi.org/10.1023/A:1012259529167

Chan, A.C., D.Y. Li, M.J. Berg, and K.J. Whitehead. 2010. Recent insights into cerebral cavernous malformations: animal models of CCM and the human phenotype. *FEBS J.* 277:1076–1083. http://dx.doi.org/10.1111/j.1742-4658.2009.07536.x

Collaborative Computational Project, Number 4. 1994. The CCP4 suite: programs for protein crystallography. *Acta Crystallogr. D Biol. Crystallogr.* 50:760–763. http://dx.doi.org/10.1107/S0907444994003112

Davis, I.W., L.W. Murray, J.S. Richardson, and D.C. Richardson. 2004. MOLPROBITY: structure validation and all-atom contact analysis for nucleic acids and their complexes. *Nucleic Acids Res.* 32:W615-W619. http://dx.doi.org/10.1093/nar/gkh398

Draheim, K.M., O.S. Fisher, T.J. Boggon, and D.A. Calderwood. 2014. Cerebral cavernous malformation proteins at a glance. *J. Cell Sci.* 127:701–707. http://dx.doi.org/10.1242/jcs.138388

Emsley, P., and K. Cowtan. 2004. Coot: model-building tools for molecular graphics. *Acta Crystallogr. D Biol. Crystallogr.* 60:2126–2132. http://dx.doi.org/10.1107/S0907444904019158

Faurobert, E., C. Rome, J. Lisowska, S. Manet-Dupé, G. Boulday, M. Malbouyres, M. Balland, A.P. Bouin, M. Kéramidas, D. Bouvard, et al. 2013. CCM1-ICAP-1 complex controls β1 integrin-dependent endothelial contractility and fibronectin remodeling. *J. Cell Biol.* 202:545–561.

Fidalgo, M., A. Guerrero, M. Fraile, C. Iglesias, C.M. Pombo, and J. Zalvide. 2012. Adaptor protein cerebral cavernous malformation 3 (CCM3) mediates phosphorylation of the cytoskeletal proteins ezrin/radixin/moesin by mammalian Ste20-4 to protect cells from oxidative stress. *J. Biol. Chem.* 287:11556–11565. http://dx.doi.org/10.1074/jbc.M111.320259

Fisher, O.S., and T.J. Boggon. 2014. Signaling pathways and the cerebral cavernous malformations proteins: lessons from structural biology. *Cell. Mol. Life Sci.* 71:1881–1892. http://dx.doi.org/10.1007/s00018-013-1532-9

Fisher, O.S., R. Zhang, X. Li, J.W. Murphy, B. Demeler, and T.J. Boggon. 2013. Structural studies of cerebral cavernous malformations 2 (CCM2) reveal a folded helical domain at its C-terminus. *FEBS Lett.* 587:272–277. http://dx.doi.org/10.1016/j.febslet.2012.12.011

Fisher, O.S., W. Liu, R. Zhang, A.L. Stiegler, S. Ghedia, J.L. Weber, and T.J. Boggon. 2015. Structural basis for the disruption of the Cerebral Cavernous Malformations 2 (CCM2) interaction with Krev Interaction

Trapped 1 (KRIT1) by disease-associated mutations. *J. Biol. Chem.* 290: 2842–2853. http://dx.doi.org/10.1074/jbc.M114.616433

Fu, C., D.R. Wehr, J. Edwards, and B. Hauge. 2008. Rapid one-step recombinational cloning. *Nucleic Acids Res.* 36:e54. http://dx.doi.org/10.1093/nar/gkn167

Girish, V., and A. Vijayalakshmi. 2004. Affordable image analysis using NIH Image/ImageJ. *Indian J. Cancer*. 41:47.

Gordon, J., J. Hwang, K.J. Carrier, C.A. Jones, Q.L. Kern, C.S. Moreno, R.H. Karas, and D.C. Pallas. 2011. Protein phosphatase 2a (PP2A) binds within the oligomerization domain of striatin and regulates the phosphorylation and activation of the mammalian Ste20-Like kinase Mst3. *BMC Biochem.* 12:54. http://dx.doi.org/10.1186/1471-2091-12-54

Goudreault, M., L.M. D'Ambrosio, M.J. Kean, M.J. Mullin, B.G. Larsen, A. Sanchez, S. Chaudhry, G.I. Chen, F. Sicheri, A.I. Nesvizhskii, et al. 2009. A PP2A phosphatase high density interaction network identifies a novel striatin-interacting phosphatase and kinase complex linked to the cerebral cavernous malformation 3 (CCM3) protein. *Mol. Cell. Proteomics*. 8:157–171. http://dx.doi.org/10.1074/mcp.M800266-MCP200

Hoellerer, M.K., M.E. Noble, G. Labesse, I.D. Campbell, J.M. Werner, and S.T. Arold. 2003. Molecular recognition of paxillin LD motifs by the focal adhesion targeting domain. *Structure*. 11:1207–1217. http://dx.doi.org/10.1016/j.str.2003.08.010

Hogan, B.M., J. Bussmann, H. Wolburg, and S. Schulte-Merker. 2008. ccm1 cell autonomously regulates endothelial cellular morphogenesis and vascular tubulogenesis in zebrafish. *Hum. Mol. Genet.* 17:2424–2432. http://dx.doi.org/10.1093/hmg/ddn142

Jones, M.K., I.J. Sarfeh, and A.S. Tarnawski. 1998. Induction of in vitro angiogenesis in the endothelial-derived cell line, EA hy926, by ethanol is mediated through PKC and MAPK. *Biochem. Biophys. Res. Commun.* 249:118–123. http://dx.doi.org/10.1006/bbrc.1998.9095

Kean, M.J., D.F. Ceccarelli, M. Goudreault, M. Sanches, S. Tate, B. Larsen, L.C. Gibson, W.B. Derry, I.C. Scott, L. Pelletier, et al. 2011. Structure-function analysis of core STRIPAK Proteins: a signaling complex implicated in Golgi polarization. *J. Biol. Chem.* 286:25065–25075. http://dx.doi.org/10.1074/jbc.M110.214486

Kemp, H.A., and G.F. Sprague Jr. 2003. Far3 and five interacting proteins prevent premature recovery from pheromone arrest in the budding yeast *Saccharomyces cerevisiae*. *Mol. Cell. Biol.* 23:1750–1763. http://dx.doi.org/10.1128/MCB.23.5.1750-1763.2003

Kiema, T., Y. Lad, P. Jiang, C.L. Oxley, M. Baldassarre, K.L. Wegener, I.D. Campbell, J. Ylänne, and D.A. Calderwood. 2006. The molecular basis of filamin binding to integrins and competition with talin. *Mol. Cell*. 21:337–347. http://dx.doi.org/10.1016/j.molcel.2006.01.011

Krissinel, E., and K. Henrick. 2007. Inference of macromolecular assemblies from crystalline state. *J. Mol. Biol.* 372:774–797. http://dx.doi.org/10.1016/j.jmb.2007.05.022

Li, X., R. Zhang, H. Zhang, Y. He, W. Ji, W. Min, and T.J. Boggon. 2010. Crystal structure of CCM3, a cerebral cavernous malformation protein critical for vascular integrity. *J. Biol. Chem.* 285:24099–24107. http://dx.doi.org/10.1074/jbc.M110.128470

Li, X., W. Ji, R. Zhang, E. Folta-Stogniew, W. Min, and T.J. Boggon. 2011. Molecular recognition of leucine-aspartate repeat (LD) motifs by the FAT-homology domain of cerebral cavernous malformation 3 (CCM3). *J. Biol. Chem.* 286:26138–26147. http://dx.doi.org/10.1074/jbc.M110.211250

Liquori, C.L., M.J. Berg, A.M. Siegel, E. Huang, J.S. Zawistowski, T. Stoffer, D. Verlaan, F. Balogun, L. Hughes, T.P. Leedom, et al. 2003. Mutations in a gene encoding a novel protein containing a phosphotyrosine-binding domain cause type 2 cerebral cavernous malformations. *Am. J. Hum. Genet.* 73:1459–1464. http://dx.doi.org/10.1086/380314

Lulo, J., S. Yuzawa, and J. Schlessinger. 2009. Crystal structures of free and ligand-bound focal adhesion targeting domain of Pyk2. *Biochem. Biophys. Res. Commun.* 383:347–352. http://dx.doi.org/10.1016/j.bbrc.2009.04.011

McCoy, A.J., R.W. Grosse-Kunstleve, P.D. Adams, M.D. Winn, L.C. Storoni, and R.J. Read. 2007. Phaser crystallographic software. *J. Appl. Cryst.* 40:658–674. http://dx.doi.org/10.1107/S0021889807021206

McNicholas, S., E. Potterton, K.S. Wilson, and M.E. Noble. 2011. Presenting your structures: the CCP4mg molecular-graphics software. *Acta Crystallogr. D Biol. Crystallogr.* 67:386–394. http://dx.doi.org/10.1107/S0907444911007281

Murshudov, G.N., P. Skubák, A.A. Lebedev, N.S. Pannu, R.A. Steiner, R.A. Nicholls, M.D. Winn, F. Long, and A.A. Vagin. 2011. REFMAC5 for the refinement of macromolecular crystal structures. *Acta Crystallogr. D Biol. Crystallogr.* 67:355–367. http://dx.doi.org/10.1107/S0907444911001314

Otwinowski, Z., and W. Minor. 1997. Processing of X-ray diffraction data collected in oscillation mode. *Methods Enzymol.* 276:307–326. http://dx.doi.org/10.1016/S0076-6879(97)76066-X

Riant, F., F. Bergametti, H.D. Fournier, F. Chapon, S. Michalak-Provost, M. Cecillon, P. Lejeune, H. Hosseini, C. Choe, M. Orth, et al. 2013. CCM3 mutations are associated with early-onset cerebral hemorrhage and multiple meningiomas. *Mol. Syndromol*. 4:165–172.

Sugden, P.H., L.J. McGuffin, and A. Clerk. 2013. SOcK, MiSTs, MASK and STicKs: the GCKIII (germinal centre kinase III) kinases and their heterologous protein-protein interactions. *Biochem. J.* 454:13–30. http://dx.doi.org/10.1042/BJ20130219

Voss, K., S. Stahl, E. Schleider, S. Ullrich, J. Nickel, T.D. Mueller, and U. Felbor. 2007. CCM3 interacts with CCM2 indicating common pathogenesis for cerebral cavernous malformations. *Neurogenetics*. 8:249–256. http://dx.doi.org/10.1007/s10048-007-0098-9

Wüstehube, J., A. Bartol, S.S. Liebler, R. Brütsch, Y. Zhu, U. Felbor, U. Sure, H.G. Augustin, and A. Fischer. 2010. Cerebral cavernous malformation protein CCM1 inhibits sprouting angiogenesis by activating DELTA-NOTCH signaling. *Proc. Natl. Acad. Sci. USA*. 107:12640–12645. http://dx.doi.org/10.1073/pnas.1000132107

Zheng, X., C. Xu, A.O. Smith, A.N. Stratman, Z. Zou, B. Kleaveland, L. Yuan, C. Didiku, A. Sen, X. Liu, et al. 2012. Dynamic regulation of the cerebral cavernous malformation pathway controls vascular stability and growth. *Dev. Cell*. 23:342–355. http://dx.doi.org/10.1016/j.devcel.2012.06.004